(Received 6 July 2025, Accepted 22 October 2025, Scheduled 22 November 2025)

An Adaptive DTC-SVM Control for Five-Phase Machines under One Open-Phase Fault

Mohamed C. Madaoui[1,2], Abdelfattah Hoggui[2,3,*], Ali Benachour[2,4], Lotfi Kerchich[4], Meriem I. Bazzine[4], Mohand O. Mahmoudi[2], and Mohamed Tadjine[1,2]

[1]*Department of Automation, Ecole Nationale Polytechnique, El Harrach, Algiers, Algeria*
[2]*Process Control Laboratory (PCL), Ecole Nationale Polytechnique, El Harrach, Algiers, Algeria*
[3]*Electrotechnical Research Laboratory (ERL), Ecole Nationale Polytechnique, El Harrach, Algiers, Algeria*
[4]*Department of Electrical Engineering, ENSTA, Algiers, Algeria*

ABSTRACT: This paper presents an adaptive Direct Torque Control with Space Vector Modulation (DTC-SVM) strategy for a five-phase induction machine fed by a two-level inverter, designed to tolerate single open-phase faults. Under such fault conditions, the five-phase inverter generates only 16 voltage vectors distributed across 8 sectors, requiring a reconfiguration of the DTC-SVM control scheme. The proposed method introduces a modified vector selection and sector allocation approach tailored to faulted operation, enabling reliable performance without extensive controller redesign. Simulation studies in MATLAB/Simulink and experimental validation on a 3.5 kW five-phase induction motor confirm the effectiveness of the proposed approach. The results show that the adaptive DTC-SVM reduces torque ripple, maintains stable flux and current waveforms, and preserves fast dynamic response during sudden load changes. In addition, the method remains straightforward to implement, combining the simplicity of DTC with the improved voltage utilization of SVM.

1. INTRODUCTION

Multiphase machines have gained significant importance in recent years over conventional three-phase machines [1], due to their inherent benefits, such as higher robustness, lower current per phase, higher power density, lower torque ripple, and greater degrees of freedom than their three-phase counterparts [2–5]. Therefore, multiphase machines are strong candidates for demanding high-power applications such as aerospace, electric aircraft, railway traction, wind energy conversion, ship propulsion, and critical safety systems [6–9].

The major advantage of multiphase machines is their intrinsic ability to tolerate faults. They can continue operating in the presence of an open or short-circuited stator phase, making them ideal for applications requiring high reliability and redundancy [10].

In this context, several control strategies have been explored to enhance the performance of multiphase induction machines under a single open-phase fault condition [11–19]. The research by Rahman et al. investigated field-oriented control (FOC) for five-phase induction machines, focusing on maximum torque calculation and enabling operation with two open phases by adjusting the post-fault flux in [20]. Dwari and Parsa proposed an optimal fault-tolerant control technique for n-phase permanent-magnet machines, in which healthy phase currents are regulated to compensate for open-circuit faults while minimizing torque ripple and stator losses, based on instantaneous power-balance theory [21]. While these FOC-based methods provide accurate control, they rely heavily on machine parameters and require post-fault reconfiguration, which increases implementation complexity.

Alternatively, Guzman et al. conducted an experimental comparison between predictive control and power integral (PI)-resonant control strategies for the fault-tolerant operation of five-phase induction motor drives under an open-phase fault condition [22]. In parallel, Gonzalez-Prieto et al. initially proposed a fault-tolerant model predictive control (MPC) using virtual voltage vectors for open-loop regulation of x-y currents, removing the need for fault detection [23]. A subsequent study focused on the implementation of an efficient model predictive control approach that leverages virtual voltage vectors (VVs) to regulate the x-y subspace currents in open-loop mode, enhancing system reliability through "natural fault tolerance" [24]. Despite their advantages, predictive control strategies often involve high computational burden and tuning complexity, which may limit their suitability for real-time applications.

Regarding direct torque control (DTC), Bermúdez et al. proposed fault-tolerant techniques using virtual vector control for five-phase induction motor drives under an open-phase fault, and they validated the approach experimentally [12]. Chikondra et al. extended the concept via theoretical analysis of the virtual vectors' effects on flux and torque, refining lookup tables and hysteresis bands [16]. An optimized switching table for DTC was also proposed in [25]. Although DTC-based methods benefit from simple structure and fast dynamics, they generally suffer from variable switching frequency and high torque ripple.

* Corresponding author: Abdelfattah Hoggui (abdelfettah.hoggui@g.enp.edu.dz).

DTC with space vector modulation (DTC-SVM) is known for its robust electrical and electromagnetic performance, constant switching frequency, and reduced sensitivity to parameter variations. However, it remains underexplored for open-phase faults in five-phase machines. The novelty of this work lies in adapting DTC-SVM to tolerate such faults by introducing a reconfigured SVM strategy together with a new transformation based on four output components. This adaptation improves flux and torque estimation under fault conditions, while preserving fast dynamic response and simplicity of implementation. In this way, the proposed approach combines the advantages of classical DTC and vector control, while addressing their main drawbacks.

This paper presents the development and evaluation of the proposed control strategy. It begins by modeling the five-phase induction motor and the two-level inverter operating under an open-phase fault condition. Following this, adaptive DTC-SVM control method is introduced. The subsequent sections detail the simulation results obtained using MATLAB/Simulink, followed by a description of the experimental setup that includes a 3.5 kW motor. Then, the experimental results are discussed. The paper concludes with a summary of the key results and insights drawn from the study.

2. MODELING OF FIVE-PHASE MACHINE UNDER ONE OPEN-PHASE FAULT

Figure 1 shows five-phase winding in healthy mode, but this work focuses on a fault condition where phase "a" is open, which causes the motor to operate with only four active stator phases (b-c-d-e). While the physical positions of the windings remain unchanged, the electrical symmetry of the machine is disrupted. As a consequence, the sum of the phase voltages no longer equals zero, as shown in Equation (1):

$$v_{sa} + v_{sb} + v_{sc} + v_{sd} + v_{se} \neq 0. \tag{1}$$

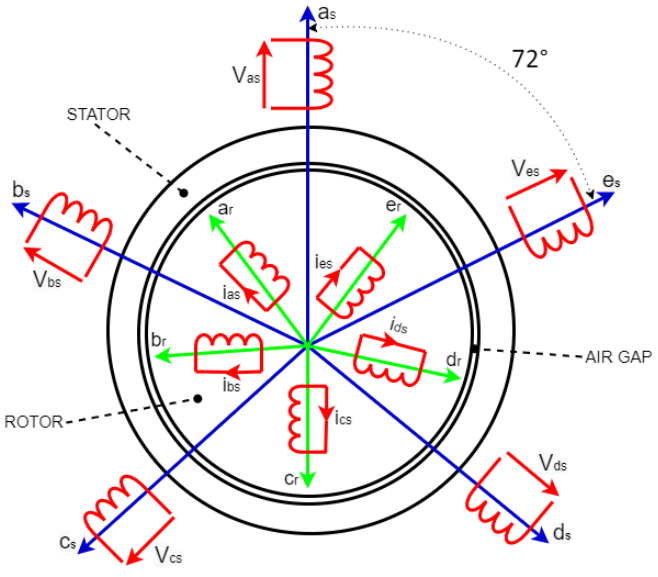

FIGURE 1. Stator winding configuration of the five-phase induction motor [26].

The open-phase condition alters the effective angular distribution of the active phases, increasing the maximum angular span between adjacent active phases to 144 electrical, compared to the uniform 72 in the healthy case. The modeling of the five-phase induction machine under one phase can be written as follows:

$$\begin{bmatrix} V_b^s \\ V_c^s \\ V_d^s \\ V_e^s \end{bmatrix} = \begin{bmatrix} r_{sb} & 0 & 0 & 0 \\ 0 & r_{sc} & 0 & 0 \\ 0 & 0 & r_{sd} & 0 \\ 0 & 0 & 0 & r_{se} \end{bmatrix} \begin{bmatrix} I_b^s \\ I_c^s \\ I_d^s \\ I_e^s \end{bmatrix} + \frac{d}{dt} \begin{bmatrix} \lambda_b^s \\ \lambda_c^s \\ \lambda_d^s \\ \lambda_e^s \end{bmatrix} \tag{2}$$

$$\begin{bmatrix} \lambda_b^s \\ \lambda_c^s \\ \lambda_d^s \\ \lambda_e^s \end{bmatrix} = \mathbf{L}_{ss} \begin{bmatrix} I_b^s \\ I_c^s \\ I_d^s \\ I_e^s \end{bmatrix} + \mathbf{M}_{sr} \begin{bmatrix} I_b^r \\ I_c^r \\ I_d^r \\ I_e^r \end{bmatrix} \tag{3}$$

$$T_e = P \cdot \begin{bmatrix} I_b^s & I_c^s & I_d^s & I_e^s \end{bmatrix} \cdot \frac{d}{d\theta} \left(\mathbf{M}_{sr} \cdot \begin{bmatrix} I_b^r \\ I_c^r \\ I_d^r \\ I_e^r \end{bmatrix} \right) \tag{4}$$

where:

$\mathbf{L}_{ss}$ and $\mathbf{L}_{rr}$ are the stator and rotor self-inductance matrices, respectively.

$\mathbf{M}_{sr}$ and $\mathbf{M}_{rs}$ represent the mutual inductance matrices between stator and rotor windings.

These matrices account for magnetic coupling and are typically symmetric in healthy machines.

A modified Clarke transformation matrix — initially introduced in [27] and shown in Equation (5) — is employed. This matrix integrates a phase shift adjustment (using $+0.25$ angular offset) to effectively realign the system dynamics. As a result, it enables the reconstruction of a symmetrical post-fault model for the five-phase machine. This transformation ensures that the stator current trajectories remain circular in the α-β plane and that the same set of equations in the α-β-x-y coordinates is preserved across both healthy and fault scenarios.

$$[C_{\text{POST}}] = \frac{2}{5} \cdot \begin{bmatrix} \cos(\vartheta) + 0.25\cos(2\vartheta) + 0.25\cos(3\vartheta) + 0.25\cos(4\vartheta) + 0.25 \\ \sin(\vartheta) \quad \sin(2\vartheta) \quad \sin(3\vartheta) \quad \sin(4\vartheta) \\ \sin(2\vartheta) \quad \sin(4\vartheta) \quad \sin(6\vartheta) \quad \sin(8\vartheta) \\ 1 \quad 1 \quad 1 \quad 1 \end{bmatrix}. \tag{5}$$

Moreover, the disconnection of phase "a" enforces $i_a = 0$, effectively removing one degree of freedom from the system. In transformed α — reference frame, this constraint appears as a linear dependence between the corresponding current components:

$$i_{sa} = 0 \;\Rightarrow\; i_\alpha + i_x = 0 \;\Rightarrow\; i_x = -i_\alpha. \tag{6}$$

Therefore, by applying the modified matrix, stator equations are reformulated in the α-β-x-y-0 coordinate system. This

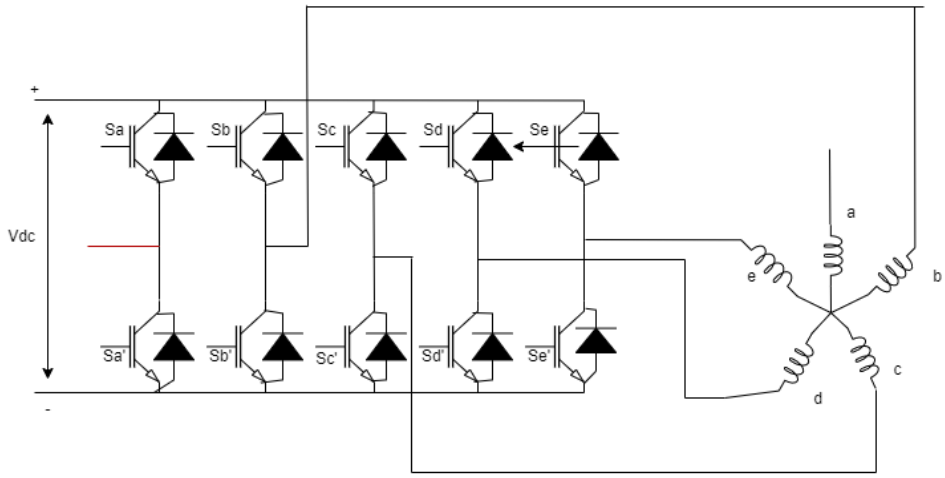

FIGURE 2. Schematic of the five-phase two-level voltage source inverter under an open-phase fault.

representation simplifies the model by yielding constant, time-invariant coefficients [27].

The corresponding stator voltages in the stationary reference frame are given by:

$$\begin{cases} v_{\alpha s} = R_s i_{\alpha s} + \dfrac{d\lambda_{\alpha s}}{dt} \\ v_{\beta s} = R_s i_{\beta s} + \dfrac{d\lambda_{\beta s}}{dt} \\ v_{xs} = R_s i_{xs} + \dfrac{d\lambda_{xs}}{dt} = R_s i_{xs} + L_{ls}\dfrac{di_{xs}}{dt} \\ v_{ys} = R_s i_{ys} + \dfrac{d\lambda_{ys}}{dt} = R_s i_{ys} + L_{ls}\dfrac{di_{ys}}{dt} \\ v_{0s} = R_s i_{0s} + \dfrac{d\lambda_{0s}}{dt} = R_s i_{0s} + L_{ls}\dfrac{di_{0s}}{dt} \end{cases} \tag{7}$$

The corresponding stator flux linkages in the stationary reference frame are given by:

$$\begin{cases} \lambda_{\alpha s} = (L_{ls} + L_m) i_{\alpha s} + L_m i_{\alpha r} \\ \lambda_{\beta s} = (L_{ls} + L_m) i_{\beta s} + L_m i_{\beta r} \\ \lambda_{xs} = L_{ls} i_{xs} \\ \lambda_{ys} = L_{ls} i_{ys} \\ \lambda_{0s} = L_{ls} i_{0s} \end{cases} \tag{8}$$

$$T_e = p(\lambda_{\alpha s} i_{\beta s} - \lambda_{\beta s} i_{\alpha s}) \tag{9}$$

3. MODELING OF A TWO-LEVEL FIVE-PHASE INVERTER UNDER ONE OPEN-PHASE FAULT

A two-level five-phase voltage source inverter (VSI) is employed to supply a five-phase induction motor, as illustrated in Figure 2. The inverter consists of five legs, each associated with a corresponding phase of the motor. Each leg contains two insulated-gate bipolar transistor (IGBT) switches: one high-side switch and one low-side switch, denoted as S_a, S_b, S_c, S_d, S_e and $S'_a, S'_b, S'_c, S'_d, S'_e$, respectively. These switches are operated in a complementary manner to prevent shoot-through faults across the DC link and to maintain proper current flow to the motor.

The inverter is powered by a constant DC voltage source V_{dc}. Under a single open-phase fault condition, the number of functional legs is reduced to four, resulting in $2^4 = 16$ possible switching states. These states generate 16 voltage space vectors, which include two zero vectors and fourteen active vectors. These vectors are distributed over eight sectors of 45 each and are used in the control strategy to maintain torque regulation and robust performance under fault conditions, as shown in Figure 3.

In the event of a one open-phase fault — assumed here to affect phase "a" — the mathematical model of the two-level five-phase inverter must be adapted to reflect the loss of one leg. The switching state S_a is excluded from the formulation, reducing the system to four active phases. The leg voltages relative to the load neutral can be expressed as [28]:

$$\begin{bmatrix} v_{bs} \\ v_{cs} \\ v_{ds} \\ v_{es} \end{bmatrix} = \frac{V_{\text{dc}}}{4} \begin{bmatrix} 3 & -1 & -1 & -1 \\ -1 & 3 & -1 & -1 \\ -1 & -1 & 3 & -1 \\ -1 & -1 & -1 & 3 \end{bmatrix} \begin{bmatrix} S_b \\ S_c \\ S_d \\ S_e \end{bmatrix} \tag{10}$$

This fault-adapted model provides a systematic way to calculate the remaining leg voltages as a function of the DC link voltage V_{dc} and switching states of the remaining inverter legs. It also incorporates the effects of mutual inductance and current dynamics, making it suitable for the use in advanced fault-tolerant control strategies. The resulting space vectors are presented in Figure 3. The 16 vectors are listed in Table 1.

4. ADAPTIVE DTC-SVM CONTROL

In this paper, a closed-loop Direct Torque Control strategy combined with Space Vector Modulation (DTC-SVM) is implemented. The corresponding block diagram is shown in Figure 4. This control method operates within the stator flux reference frame and utilizes two PI controllers to regulate the flux and

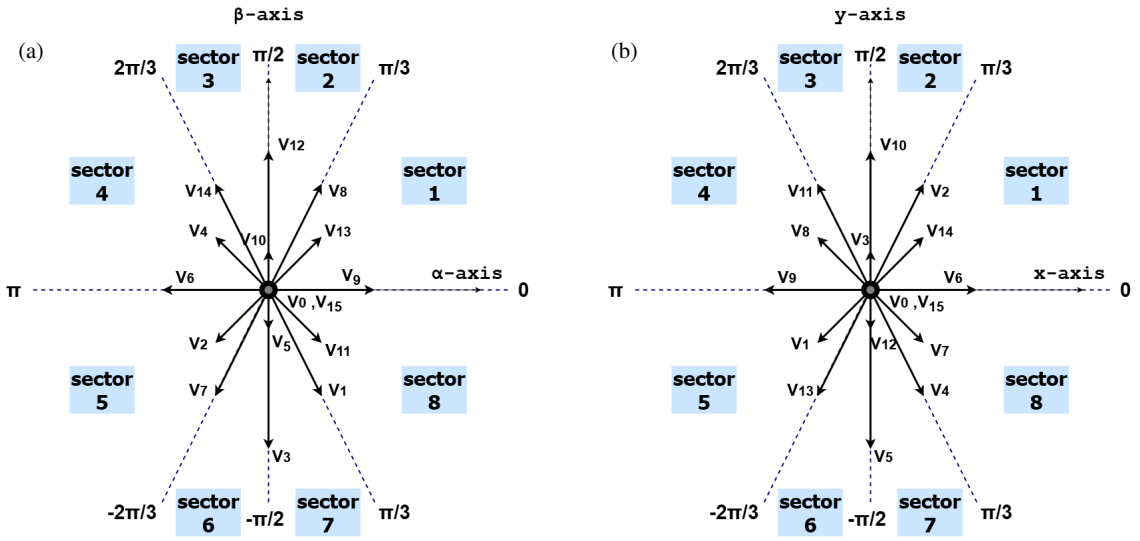

FIGURE 3. Vector distribution in (a) α-β and (b) x-y frames under an open-phase fault.

TABLE 1. The selected 16 active vectors with their switching states and output voltages in α-β and x-y frames.

Vectors	States	α-β Frame		x-y Frame	
		$\lvert V_{\text{ref}}\rvert$	θ_{out} (°)	$\lvert V_{\text{ref}}\rvert$	θ_{out} (°)
Active Vectors					
V_1	[0001]	0.39998	−59.5	0.39999	−133.56
V_2	[0010]	0.39999	−133.56	0.39998	59.5
V_3	[0100]	0.64718	−90	0.24721	90
V_4	[1000]	0.39999	133.56	0.39998	−59.5
V_5	[0011]	0.24721	−90	0.64718	−90
V_6	[0110]	0.64720	180	0.24720	0
V_7	[0111]	0.64719	−120.44	0.24720	−46.43
V_8	[1001]	0.39998	59.5	0.39999	133.56
V_9	[1010]	0.24720	0	0.64720	180
V_{10}	[1100]	0.24721	90	0.64718	90
V_{11}	[1101]	0.24720	46.43	0.64719	120.44
V_{12}	[1110]	0.64718	90	0.24721	−90
V_{13}	[1011]	0.24720	46.43	0.64719	−120.44
V_{14}	[1110]	0.64719	120.44	0.24720	46.43
Zero Vectors					
V_0	[0000]	0	0	0	0
V_{31}	[1111]	0	0	0	0

torque independently. The reference voltages in the d-q frame are calculated using the following expressions [29]:

$$\begin{cases} V_{ds} = R_s i_{ds} + \frac{d\lambda_s}{dt} \\ V_{qs} = R_s i_{qs} + \omega \lambda_s \end{cases} \tag{11}$$

and the electromagnetic torque is calculated by:

$$T_e = p\lambda_s i_{qs} \tag{12}$$

Once the reference voltages are obtained, they are transformed into the stationary α-β reference frame. This transformation allows the SVM to synthesize the appropriate voltage vector needed for control.

In this approach, a two-vector space vector modulation method is used. This technique selects the two longest vectors within each sector to approximate the desired reference voltage vector.

As mentioned in the previous section, under an open-phase fault condition, the number of available space vectors is reduced to 16. Notably, vectors that appear short in the α-β frame — such as vectors 10, 5, 11, 13, 4, and 2, become long vectors in the x-y frame. Due to their tendency to introduce considerable torque ripple and mechanical vibrations, these vectors were deliberately excluded from our implementation.

At each instant, the reference vector lies between two adjacent vectors V_a and V_b, which are separated by an angle of $\pi/3$ or $\pi/6$. Together with zero vector V_0 at the center, the reference vector is synthesized using two-vector SVM according to:

$$V_s = d_a V_a + d_b V_b + d_0 V_0, \tag{13}$$

where d_a, d_b, and d_0 are the respective duty cycles given by:

$$d_a = m_v \sin\left(\frac{\pi}{4} - \theta_{\text{out}}\right), \tag{14}$$

$$d_b = m_v \sin\left(\theta_{\text{out}}\right), \tag{15}$$

$$d_0 = 1 - d_a - d_b, \tag{16}$$

The modulation index m_v and $|V_l|$ are defined as:

$$m_v = \frac{|V_s|}{|V_l| \sin\left(\frac{\pi}{4}\right)}, \tag{17}$$

$$|V_l| = \left(\frac{3}{4}\right) \cos\left(\frac{\pi}{4}\right) U_{pn}, \tag{18}$$

with $0 < \theta_{\text{out}} \leq \pi/3$.

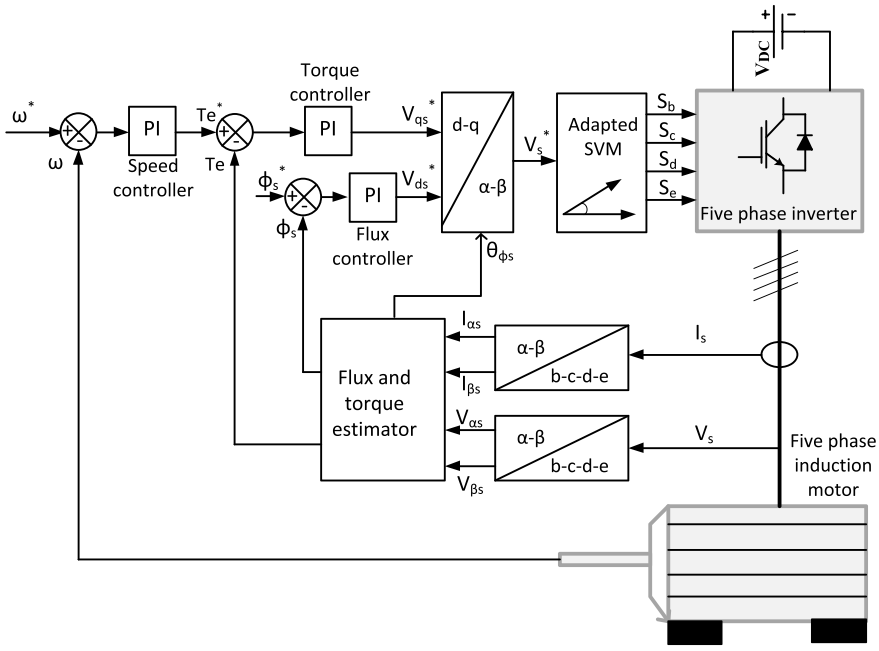

FIGURE 4. Block diagram of DTC-SVM [26].

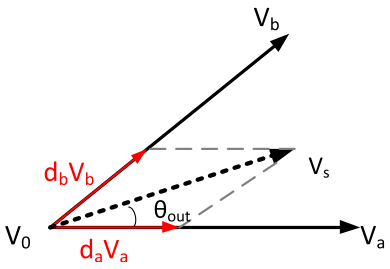

FIGURE 5. Reference voltage vector and its projection.

In Figure 5, a reference vector and its projection are presented.

By analogy to the healthy condition, the switching durations are determined by:

$$t_a = \frac{|V_s| \cdot \sin\left(k\frac{\pi}{4} - \alpha\right)}{|V_l| \cdot \sin\left(\frac{\pi}{4}\right)}, \tag{19}$$

$$t_b = \frac{|V_s| \cdot \sin\left(\alpha - (k-1)\frac{\pi}{4}\right)}{|V_l| \cdot \sin\left(\frac{\pi}{4}\right)}, \tag{20}$$

$$t_0 = T_s - t_a - t_b. \tag{21}$$

where:

- T_s is the switching period;
- α is the angle of the reference vector in the $(\alpha$-$\beta)$ plane;
- $|V_s|$ is the magnitude of the reference vector;
- k is the index of the current sector.

In the simulation studies, the PI controllers were initially tuned using the Ziegler-Nichols method, followed by minor manual adjustments to improve dynamic response and stability.

For the experimental implementation, the same Ziegler-Nichols approach was adopted as the starting point. However, due to the differences between the simulated model and physical system, a trial-and-error (tâtonnement) procedure was applied to refine the controller gains and achieve accurate performance under real operating conditions.

5. SIMULATION RESULTS

To evaluate the effectiveness of the proposed adaptive DTC-SVM control strategy for the five-phase induction motor under a single open-phase fault condition, simulations were conducted to assess both static and dynamic performances. The static performance was analyzed using key indicators such as torque ripple and the Total Harmonic Distortion (THD) of stator currents. Meanwhile, the dynamic behavior was evaluated by observing the system's response to reference speed variations, focusing on metrics including response time, overshoot, and overall stability.

The parameters of the 3.5 kW five-phase induction machine used in both the simulation and experimental setup are summarized in Table 2.

TABLE 2. Parameters of the five-phase induction machine used in the study.

Parameter	Value
pole pairs Number	1
R_s	9.5 Ω
R_r	7.3 Ω
L_s	1.389 H
L_r	1.331 H
L_m	1.323 H
P_{nom}	3.5 KW
T_{nom}	12.7 N·m

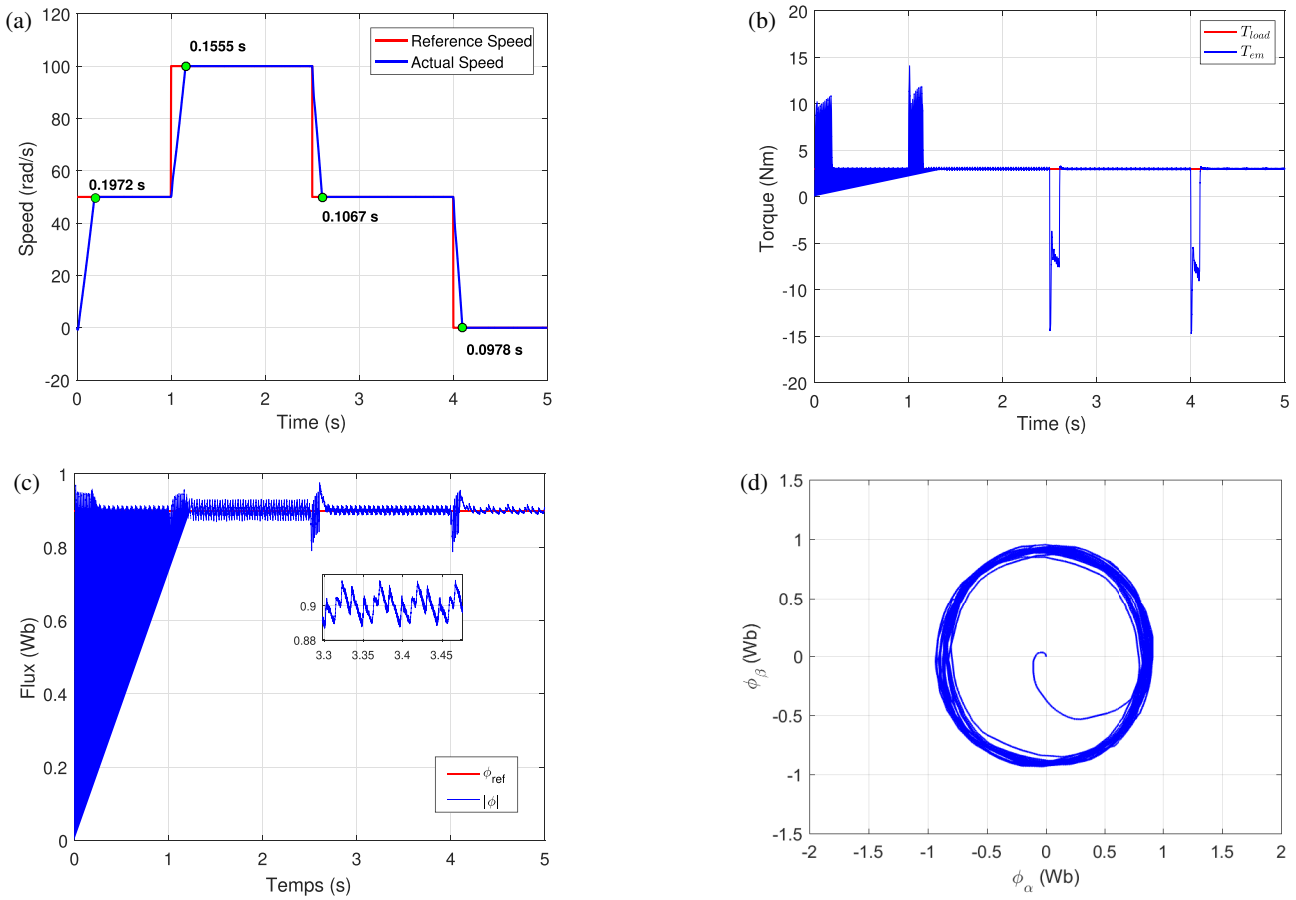

FIGURE 6. Simulation results of electromagnetic parameters in Test 1. (a) Speed response. (b) Electromagnetic torque. (c) Flux magnitude. (d) Flux trajectory.

Test 1 applies a reference speed that increases from 0 rad/s to 100 rad/s, then decreases back to 0 rad/s in steps of 50 rad/s. In Test 2, the speed reference begins at 100 rad/s and decreases stepwise by 50 rad/s down to −100 rad/s. Both tests are conducted under a constant torque load.

In Figures 6(a) and 7(a), the actual rotor speed accurately tracks the reference, exhibiting minimal steady-state error. In Test 1, the rise time during transitions reaches approximately 0.15 s when going from 50 rad/s to 100 rad/s, and 0.01 s when going from 50 rad/s to 0 rad/s. In Test 2, the rise time is about 0.10 s when the speed changes from 100 rad/s to 50 rad/s, and 0.08 s from −50 rad/s to −100 rad/s when reversing motor direction. No significant overshoot is observed, indicating good dynamic performance and high control precision.

Figures 6(b) and 7(b) illustrate the electromagnetic torque response. It closely follows its reference in both tests during speed transients. Short-duration peaks appear in the torque. In Test 1, they reach up to 11 N·m, while in Test 2, they rise to approximately 14 N·m at 2.5 s. Additionally, the maximum steady-state torque ripple remains around 0.04 N·m.

Figures 6(c) and 7(c) show the stator flux magnitude. The flux remains close to the desired reference value of 0.9 Wb. A maximum flux ripple about 0.028 Wb is observed in steady state for both tests, forming an almost circular trajectory, as illustrated in Figures 6(d) and 7(d).

Figures 8(a) and 8(b) present the stator current waveforms for Test 1 and Test 2, respectively. During the transient state, the peak current was approximately 7 A for both tests.

Figures 9(a) and 9(b) illustrate the stator current and its fast Fourier transform (FFT) spectrum. The Total Harmonic Distortion (THD) is approximately 11.08%. Finally, Figure 9(c) shows the inverter output voltage waveform, and its FFT spectrum is presented in Figure 9(d), which has a THD value of 111.28%.

6. EXPERIMENTAL SETUP

Figure 10 depicts the experimental arrangement designed to validate and implement the proposed adaptive DTC-SVM strategy on a five-phase induction motor rated at 3.5 kW. The test bench consists of two main sections: power section and control section [26].

The power section consists of a 3.5 kW five-phase induction motor mechanically connected to a DC generator serving as a variable load. The generator is linked to adjustable resistors, which allow the load torque to be modified by changing the resistance. Power to the motor is supplied by two Semikron three-phase inverters, fed by a constant 450 V DC bus obtained through a diode rectifier connected to an autotransformer.

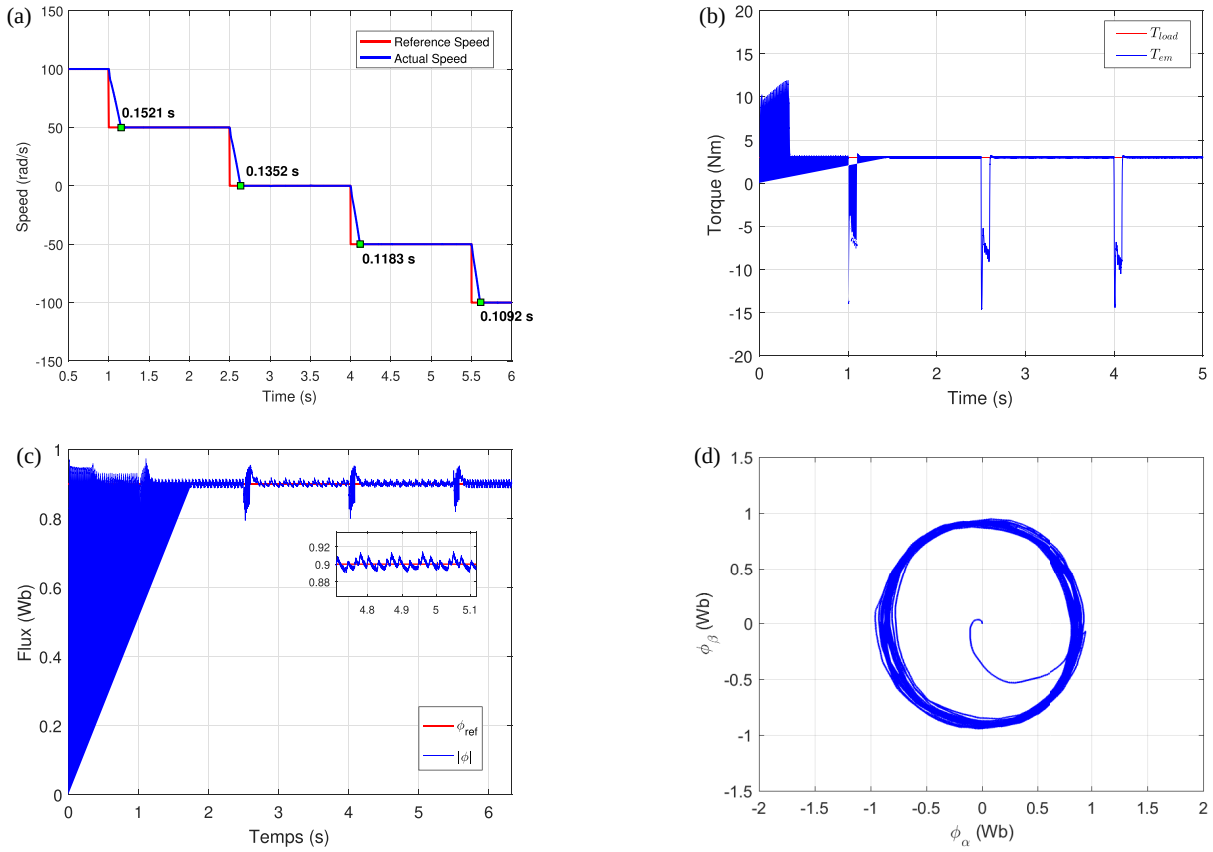

FIGURE 7. Simulation results of electromagnetic parameters in Test 2. (a) Speed response. (b) Electromagnetic torque. (c) Flux magnitude. (d) Flux trajectory.

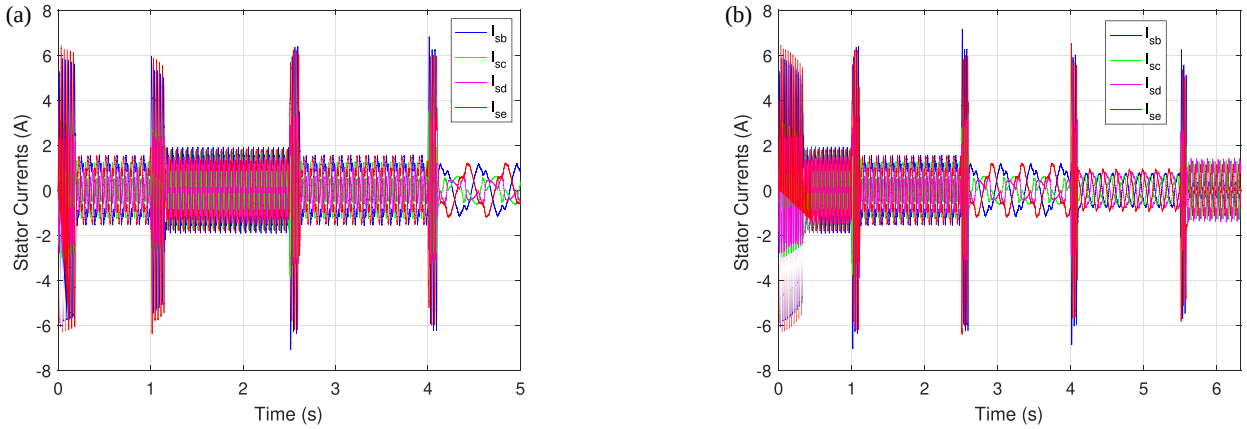

FIGURE 8. Stator current waveforms. (a) Test 1. (b) Test 2.

The control section is based on a DS1104 controller board from dSPACE GmbH, mounted in a PC. The control algorithms are developed using MATLAB/Simulink together with ControlDesk. Real-time execution is achieved through Simulink's Real-Time Interface toolbox, with the generated code automatically compiled and loaded onto the DS1104 board using ControlDesk Manager. ControlDesk also provides an interactive platform for adjusting signals and monitoring system behavior in real time.

A dSPACE CLP1104 connector panel ensures proper signal exchange between the control and power stages. Furthermore, the setup includes an interface for conditioning control signals and a measurement system equipped with various sensors. The measurement setup uses an incremental encoder to capture speed and Hall-effect LEM sensors to measure currents.

7. EXPERIMENTAL RESULTS

To validate the simulation results, an experimental evaluation was conducted. This section presents the results obtained from testing the proposed adaptive DTC-SVM control applied to a five-phase induction motor under different operating scenarios.

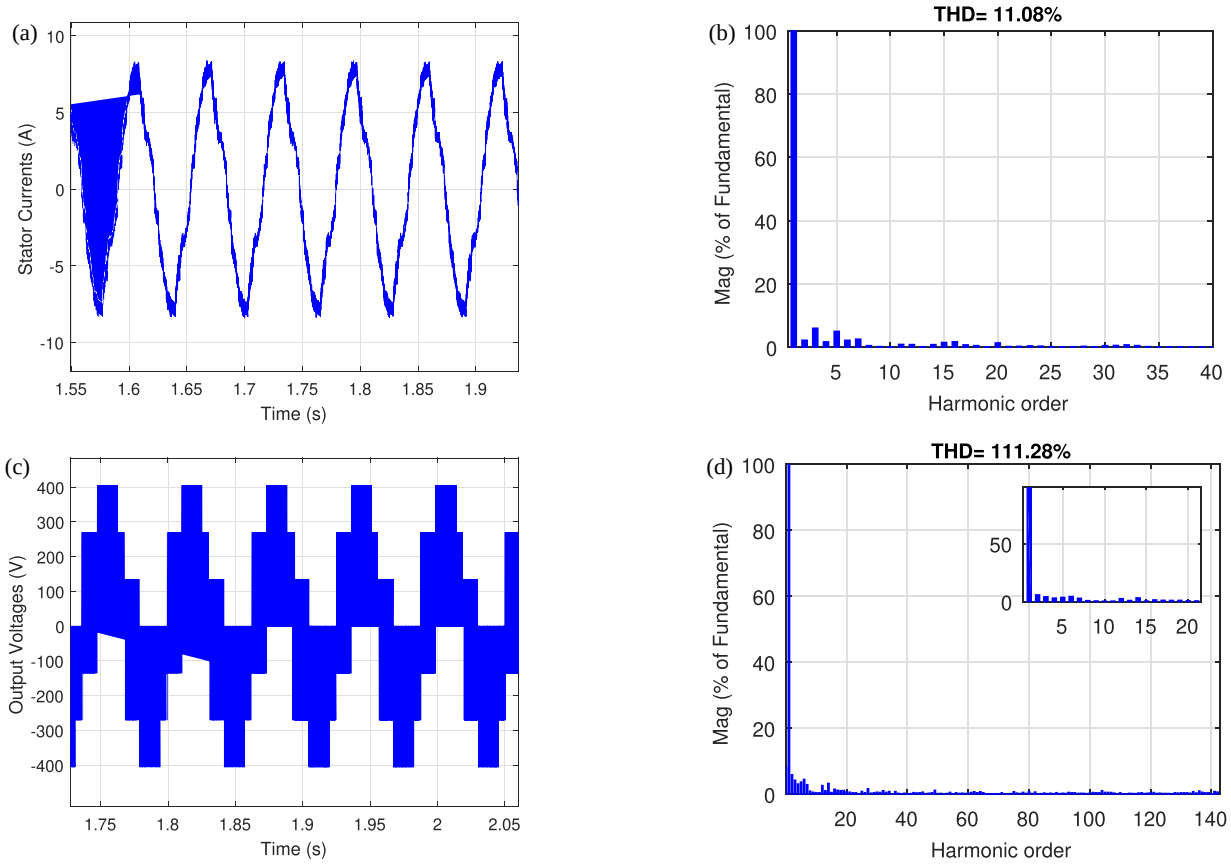

FIGURE 9. Simulation results of electrical parameters. (a) Zoomed phase current. (b) Current FFT. (c) Inverter voltages. (d) Voltage FFT.

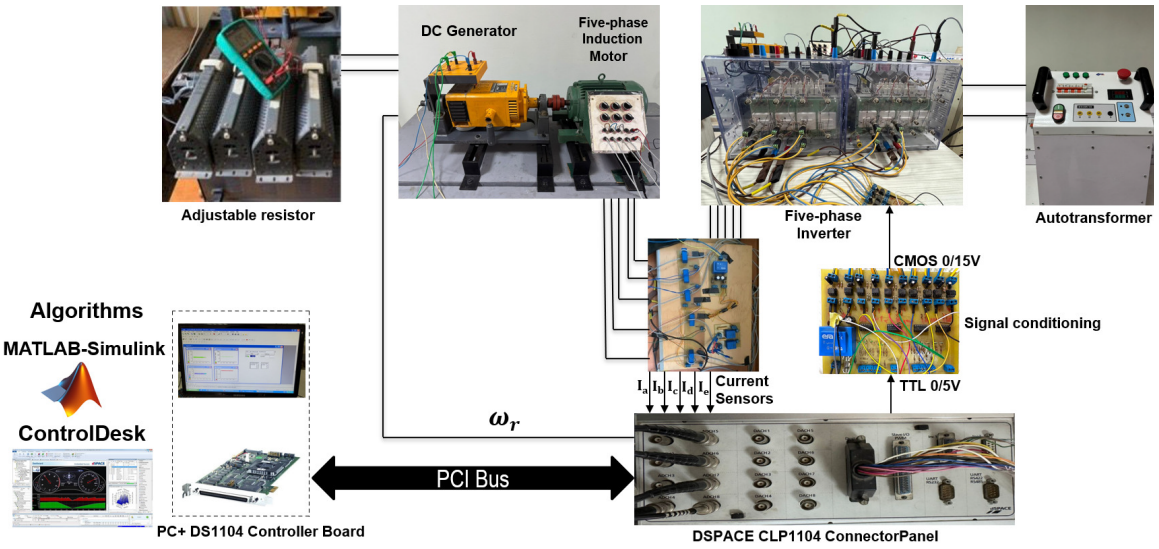

FIGURE 10. Diagram of the experimental setup.

Performance was assessed through same steady-state and transient behavior analysis as in simulations.

Figures 11 and 12 display mechanical and electromagnetic variables observed during testing, including speed, torque, and stator flux. The same speed references as in the simulations were used, and both tests were performed under a constant load.

In Figures 11(a) and 12(a), the actual speed follows the reference accurately. In the first test, the response time is 1.66 seconds for acceleration from 0 to 50 rad/s and 0.92 seconds from 50 to 100 rad/s. During deceleration, it takes 1 second from 100 to 50 rad/s and 0.78 seconds from 50 to 0 rad/s.

In contrast, the second test shows improved dynamics: 0.34 seconds for deceleration from 100 to 50 rad/s and 1.66 seconds

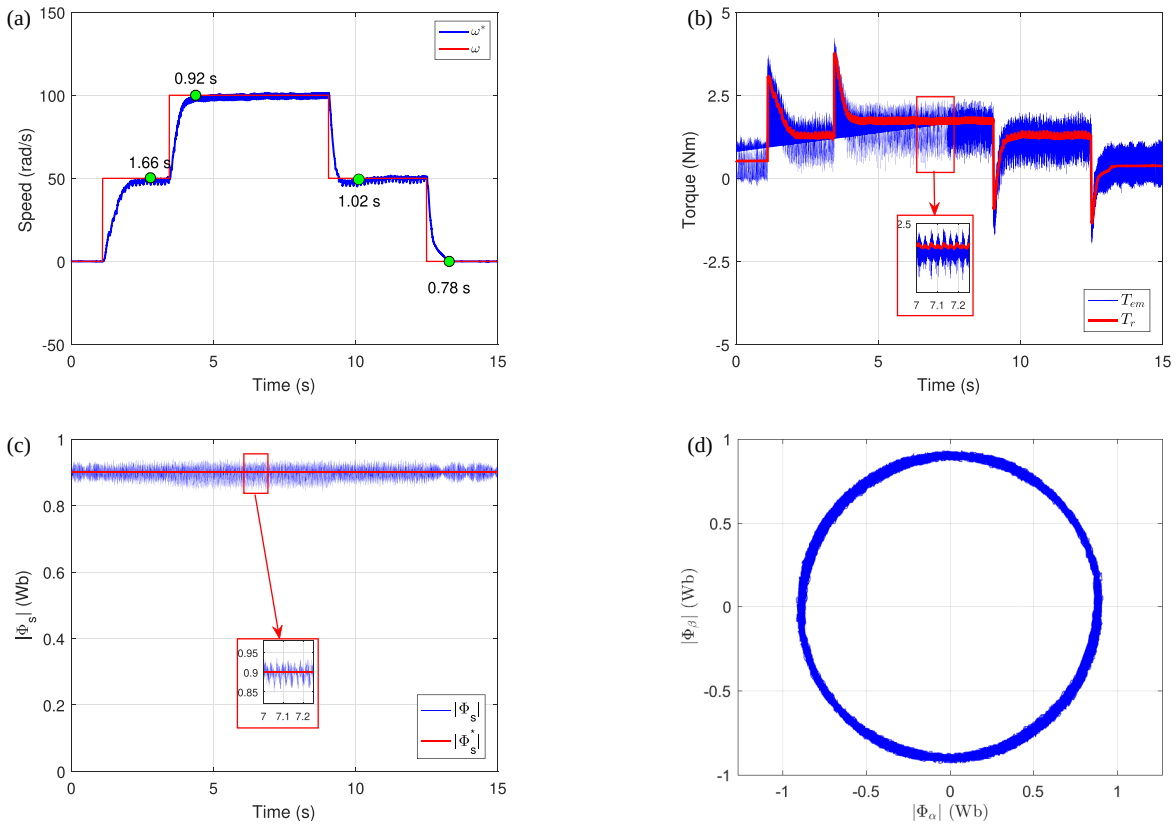

FIGURE 11. Experimental results of electromagnetic parameters. (a) Speed response. (b) Electromagnetic torque. (c) Flux magnitude. (d) Flux trajectory.

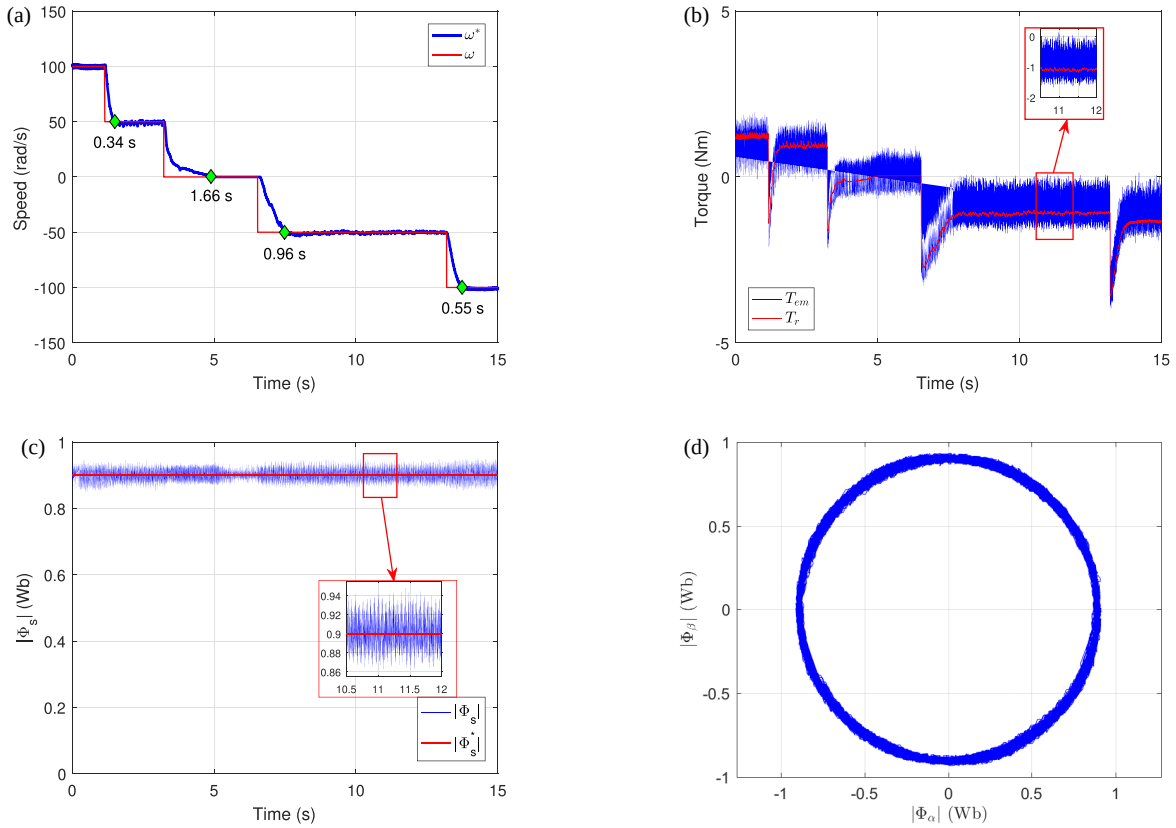

FIGURE 12. Experimental results of electromagnetic parameters. (a) Speed response. (b) Electromagnetic torque. (c) Flux magnitude. (d) Flux trajectory.

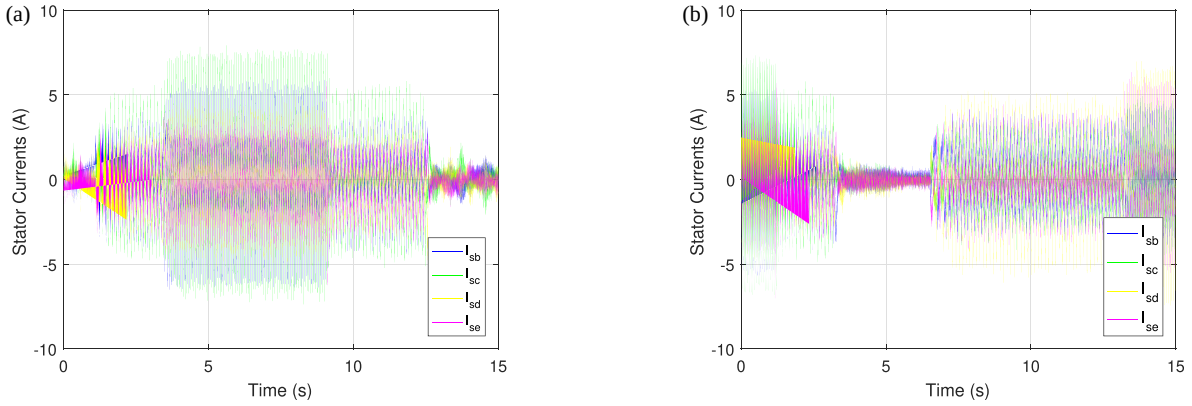

FIGURE 13. Stator currents waveform. (a) Test 1. (b) Test 2.

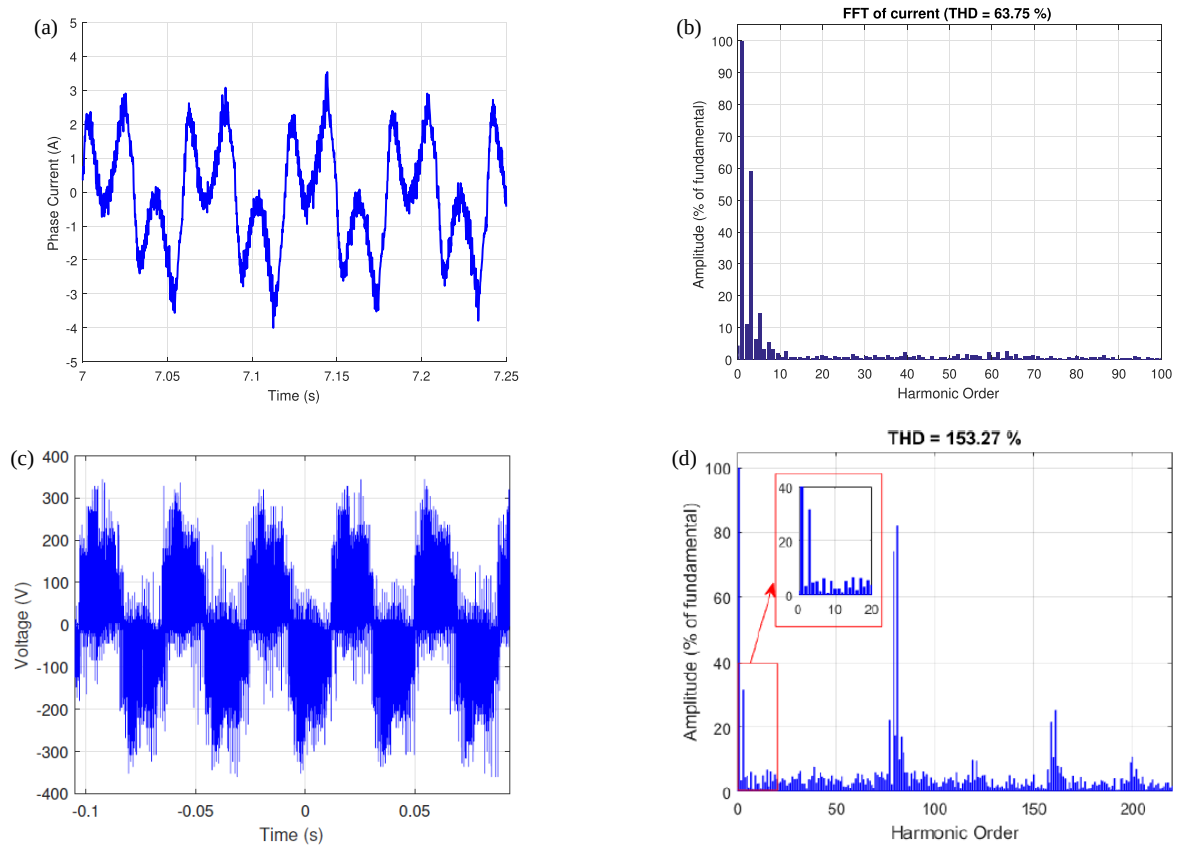

FIGURE 14. Experimental results of electrical parameters. (a) Zoomed stator phase current. (b) Stator current FFT. (c) Output voltage. (d) FFT of the output voltage.

from 50 to 0 rad/s. When reversing the motor's direction, the system reaches -50 rad/s in 0.96 seconds and -100 rad/s in 0.55 seconds.

Figures 11(b) and 12(b) show that the torque closely follows its reference in both cases. The observed torque ripple averages 0.633 Nm in the first test and 0.591 Nm in the second, attributed to the important phase shift introduced by the open-phase fault.

As shown in Figures 11(c) and 12(c), the magnitude of the stator flux remains close to its reference value, with moderate fluctuations, particularly noticeable at 100 rad/s. These cause a flux ripple of up to 0.08 Wb during the tests. The flux trajectory is circular in both tests, as illustrated in Figures 11(d) and 12(d).

Figures 13(a) and 13(b) display the stator current waveforms for Test 1 and Test 2, respectively. As the speed increases, both the magnitude and frequency of the stator currents increase and vice versa. During the transient state, peak current values reach 7.2 A in Test 1 and 6.9 A in Test 2.

Figures 14(a) and 14(b) illustrate the stator current and its FFT spectrum at 100 rad/s. The Total Harmonic Distortion (THD) is approximately 63.75%. Figure 14(c) illustrates the inverter output voltage waveform at a speed of 100 rad/s. The waveform is periodic but more variable, exhibiting a high harmonic content. As shown in Figure 14(d), THD reaches 153.27%.

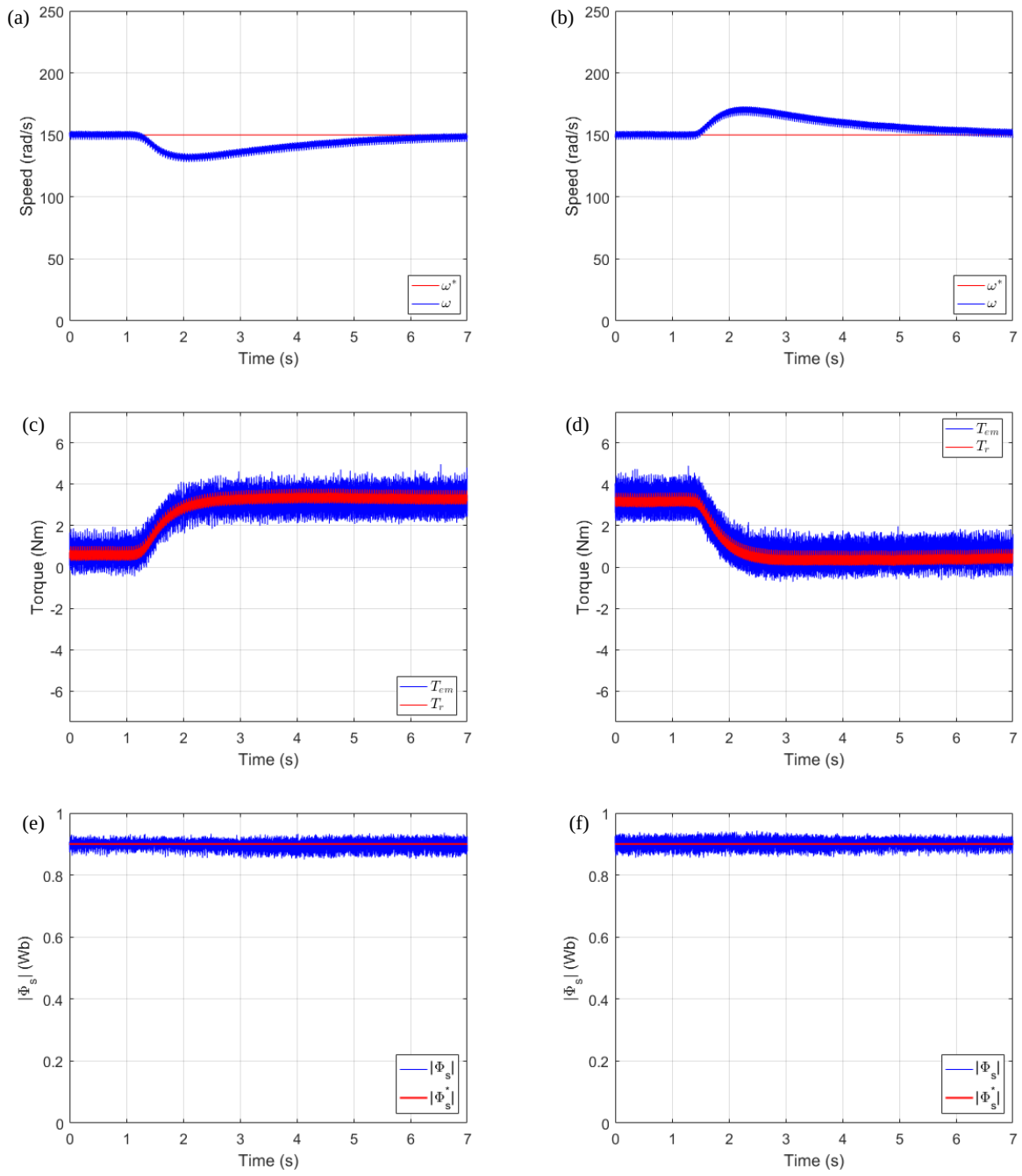

FIGURE 15. Experimental results of the electromagnetic parameters when a resistive load is introduced (a, c, e) or removed (b, d, f). (a) Speed response to loading. (b) Speed response to unloading. (c) Electromagnetic torque at loading. (d) Electromagnetic torque at unloading. (e) Stator flux magnitude at loading. (f) Stator flux magnitude at unloading.

Figures 15(a) and (b) show the rotor speed response to a change in resistive torque. In Figure 15(a), the speed decreases slightly by about 20 rad/s, and the machine takes approximately 4.73 s to restabilize at the reference speed once the load is applied. In Figure 15(b), the speed increases slightly by around 20 rad/s, and the recovery time to the reference speed is about 4.34 s.

Figures 15(c) and (d) present the electromagnetic torque response. In Figure 15(c), the torque rises at 1.27 s by 2.9 N·m, with a steady ripple about 1.2 N·m throughout the test. In Figure 15(d), the torque decreases at 1.5 s by 2.75 N·m, accompanied by a steady ripple of nearly 2 N·m.

Figures 15(e) and 15(f) illustrate the stator flux behavior. In Figure 15(e), the flux ripple increases from 0.05 Wb to 0.07 Wb under load. In Figure 15(f), the flux ripple decreases from 0.06 Wb to 0.05 Wb once the load is removed.

The experimental results shown in Figures 11 to 15 highlight the effectiveness of the control strategy over different operating conditions. The machine maintains stable operation, with the observed variations in speed, torque, and flux ripple remaining within acceptable limits.

TABLE 3. The experimental results of Test 1 and Test 2 using the adaptive DTC-SVM control strategy.

Performance Indicator	Test 1	Test 2	Comment
Response Time (speed change)	Fast	Fast	Test 2 is faster
Torque Ripple	Moderate	Moderate	Slightly lower in Test 2
Stator Flux Ripple	Low	Low	Slightly lower in Test 2
Peak Stator Current (transient)	6.9 A	7.2 A	–

TABLE 4. Comparison of DTC-SVM with two vectors under healthy and faulty conditions.

Parameter	DTC-SVM (2 vect.) healthy	DTC-SVM (2 vect.) faulty
Response time	Faster	Fast
Torque ripple	Medium	High
Flux ripple	Small	Medium
Stator current shape	Near-sinusoidal	Near-sinusoidal but with high distortion
Currents balancing	Balanced	Unbalanced
Stator current peak	2.85 A	6.9 A
Stator current THD	37.48%	63%
Voltage THD	103.88%	153%
Load change response (no-load to full-load)	Moderate drop, short recovery	Higher drop, long recovery
Load change response (full-load to no-load)	Moderate overshoot, short recovery	High overshoot, long recovery

Table 3 provides a summary of the experimental results evaluating the performance of the adaptive DTC-SVM control strategy.

Table 4 presents the observed performance differences between DTC-SVMs under healthy and faulty conditions.

8. CONCLUSION

This study investigated the performance of an adaptive DTC-SVM control strategy for a five-phase induction motor operating under a one open-phase fault. Through simulation and experimental validation, several key results were drawn regarding the system's static and dynamic behavior.

Speed Response: In both simulation and experimental tests, the motor's speed followed the reference with high accuracy, smooth transitions during acceleration, deceleration, rotation direction reversal, and resistive load introduction and removal, with stable behavior showing consistent dynamic response and negligible overshoot in most cases.

Torque Regulation: The electromagnetic torque closely followed its reference throughout the different operating scenarios, despite transient disturbances caused by abrupt speed changes, with moderate steady-state torque ripple.

Stator Flux Behavior: The stator flux magnitude remained near its desired reference value, with moderate ripple during dynamic transitions. The flux trajectory in the stationary reference frame preserved a nearly circular pattern, indicating successful flux regulation despite the phase fault.

Current Quality: Under both simulation and experimental conditions, the stator currents remained nearly stable during steady-state operation. As the speed increased, both the frequency and magnitude of the currents rose accordingly. Conversely, a decrease in speed led to a reduction in both frequency and magnitude. Despite the inherent limitations in available voltage vectors under fault conditions, the system maintained operational stability with acceptable current performance.

In summary, the adaptive DTC-SVM strategy proved to be a viable solution for fault-tolerant control of five-phase induction machines. It ensured reliable operation under an open-phase fault, maintaining satisfactory performance across speed, torque, and flux control, while offering acceptable harmonic content. This validates the effectiveness of the proposed method and highlights its potential for practical applications requiring high reliability and continuity of service under fault conditions.

Future research directions may focus on two main aspects: (i) extending the proposed approach to address more severe fault scenarios, such as two open-phase faults or multiple simultaneous faults, and (ii) integrating fault detection and diagnosis mechanisms based on artificial intelligence algorithms to enable faster and more accurate identification of fault conditions.

REFERENCES

[1] Kim, N. and M. Kim, "Modified direct torque control system of five phase induction motor," *Journal of Electrical Engineering & Technology*, Vol. 4, No. 2, 266–271, 2009.

[2] Krishnan, R., *Electric Motor Drives: Modeling, Analysis, and Control*, Prentice Hall, Upper Saddle River, NJ, USA, 2001.

[3] Magdy, M., S. Abu-Zaid, and M. A. Elwany, "Artificial intelligent techniques based on direct torque control of induction machines," *International Journal of Power Electronics and Drive Systems (IJPEDS)*, Vol. 12, No. 4, 2070–2082, 2021.

[4] Akay, A. and P. Lefley, "Torque ripple reduction method in a multiphase PM machine for no-fault and open-circuit fault-tolerant conditions," *Energies*, Vol. 14, No. 9, 2615, 2021.

[5] Shawier, A., A. S. Abdel-Khalik, R. A. Hamdy, K. H. Ahmed, and S. Ahmed, "Postfault operation of five-phase induction machine with minimum total losses under single open-phase fault," *IEEE Access*, Vol. 8, 208 696–208 706, 2020.

[6] Barrero, F. and M. J. Duran, "Recent advances in the design, modeling, and control of multiphase machines — Part I," *IEEE Transactions on Industrial Electronics*, Vol. 63, No. 1, 449–458, 2016.

[7] Levi, E., "Multiphase electric machines for variable-speed applications," *IEEE Transactions on Industrial Electronics*, Vol. 55, No. 5, 1893–1909, 2008.

[8] Bojoi, R., A. Cavagnino, A. Tenconi, and S. Vaschetto, "Multiphase PM machine for more electric aircraft applications: Prototype for design validation," in *IECON 2012 — 38th Annual Conference on IEEE Industrial Electronics Society*, 3628–3634, Montreal, QC, Canada, 2012.

[9] Shi, L.-W. and B. Zhou, "Comparative study of a fault-tolerant multiphase wound-field doubly salient machine for electrical actuators," *Energies*, Vol. 8, No. 5, 3640–3660, 2015.

[10] Salehifar, M., R. S. Arashloo, J. M. Moreno-Equilaz, V. Sala, and L. Romeral, "Fault detection and fault tolerant operation of a five phase PM motor drive using adaptive model identification approach," *IEEE Journal of Emerging and Selected Topics in Power Electronics*, Vol. 2, No. 2, 212–223, 2014.

[11] Bermúdez, M., I. González-Prieto, F. Barrero, M. J. Durán, and X. Kestelyn, "Open-phase fault operation of 5-phase induction motor drives using DTC techniques," in *IECON 2015 — 41st Annual Conference of the IEEE Industrial Electronics Society*, 595–600, Yokohama, Japan, 2015.

[12] Bermudez, M., I. Gonzalez-Prieto, F. Barrero, H. Guzman, M. J. Duran, and X. Kestelyn, "Open-phase fault-tolerant direct torque control technique for five-phase induction motor drives," *IEEE Transactions on Industrial Electronics*, Vol. 64, No. 2, 902–911, 2017.

[13] Bermúdez, M., H. Guzmán, I. González-Prieto, F. Barrero, M. J. Durán, and X. Kestelyn, "Comparative study of DTC and RFOC methods for the open-phase fault operation of a 5-phase induction motor drive," in *IECON 2015 — 41st Annual Conference of the IEEE Industrial Electronics Society*, 2702–2707, Yokohama, Japan, 2015.

[14] Guzmán, M. B., "Nouvelles techniques de commande pour les entraînements électriques polyphasés: Commande en mode instantané (DTC et MPC) dans des situations limites," Ph.D. dissertation, École Nationale Supérieure des Arts et Métiers, Universidad de Sevilla, Espagne, 2018.

[15] Kellner, J., S. Kaščák, and Z. Ferková, "Investigation of the properties of a five-phase induction motor in the introduction of new fault-tolerant control," *Applied Sciences*, Vol. 12, No. 4, 2249, 2022.

[16] Chikondra, B., U. R. Muduli, and R. K. Behera, "An improved open-phase fault-tolerant DTC technique for five-phase induction motor drive based on virtual vectors assessment," *IEEE Transactions on Industrial Electronics*, Vol. 68, No. 6, 4598–4609, 2021.

[17] Masoud, M. I., S. M. Dabour, A. E.-W. Hassan, and E. M. Rashad, "Control of five-phase induction motor under open-circuit phase fault fed by fault tolerant VSI," in *2015 IEEE 10th International Symposium on Diagnostics for Electrical Machines, Power Electronics and Drives (SDEMPED)*, 327–332, Guarda, Portugal, 2015.

[18] Habibullah, M., T. Debanath, and M. S. H. Sabbir, "Fault tolerant control of five-phase induction motor drive," in *Induction Motors*, A. El-Shahat (ed.)., Chapter 6, IntechOpen, Rijeka, 2023.

[19] Guzman, H., M. J. Duran, F. Barrero, B. Bogado, and S. Toral, "Speed control of five-phase induction motors with integrated open-phase fault operation using model-based predictive current control techniques," *IEEE Transactions on Industrial Electronics*, Vol. 61, No. 9, 4474–4484, 2014.

[20] Rahman, K., S. Rahman, M. S. Bhaskar, A. Iqbal, A. Khandakar, M. Tariq, and B. Alamri, "Field-oriented control of five-phase induction motor fed from space vector modulated matrix converter," *IEEE Access*, Vol. 10, 17 996–18 007, 2022.

[21] Dwari, S. and L. Parsa, "An optimal control technique for multiphase PM machines under open-circuit faults," *IEEE Transactions on Industrial Electronics*, Vol. 55, No. 5, 1988–1995, 2008.

[22] Guzman, H., M. J. Duran, F. Barrero, L. Zarri, B. Bogado, I. G. Prieto, and M. R. Arahal, "Comparative study of predictive and resonant controllers in fault-tolerant five-phase induction motor drives," *IEEE Transactions on Industrial Electronics*, Vol. 63, No. 1, 606–617, 2016.

[23] Gonzalez-Prieto, A., I. Gonzalez-Prieto, M. J. Duran, and F. Barrero, "Efficient model predictive control with natural fault-tolerance in asymmetrical six-phase induction machines," *Energies*, Vol. 12, No. 20, 3989, 2019.

[24] González, O., M. Ayala, C. Romero, J. Rodas, R. Gregor, L. Delorme, I. González-Prieto, M. J. Durán, and M. Rivera, "Comparative assessment of model predictive current control strategies applied to six-phase induction machines," in *2020 IEEE International Conference on Industrial Technology (ICIT)*, 1037–1043, Buenos Aires, Argentina, February 2020.

[25] Zhou, C., R. Zhong, G. Sun, D. Zhao, X. Zhao, and G. Jing, "Fault-tolerant direct torque control of five-phase permanent magnet synchronous motor under single open-phase fault based on virtual vectors," *Energies*, Vol. 17, No. 11, 2660, 2024.

[26] Hoggui, A., A. Benachour, M. C. Madaoui, and M. O. Mahmoudi, "Comparative analysis of direct torque control with space vector modulation (DTC-SVM) and finite control set-model predictive control (FCS-MPC) of five-phase induction motors," *Progress In Electromagnetics Research B*, Vol. 108, 89–104, 2024.

[27] Guzmán, H., M. J. Durán, and F. Barrero, "A comprehensive fault analysis of a five-phase induction motor drive with an open phase," in *2012 15th International Power Electronics and Motion Control Conference (EPE/PEMC)*, LS5b.3–1–LS5b.3–6, Novi Sad, Serbia, September 2012.

[28] Bermudez, M., I. Gonzalez-Prieto, F. Barrero, H. Guzman, X. Kestelyn, and M. J. Duran, "An experimental assessment of open-phase fault-tolerant virtual-vector-based direct torque control in five-phase induction motor drives," *IEEE Transactions on Power Electronics*, Vol. 33, No. 3, 2774–2784, 2018.

[29] Lai, Y.-S. and J.-H. Chen, "A new approach to direct torque control of induction motor drives for constant inverter switching frequency and torque ripple reduction," *IEEE Transactions on Energy Conversion*, Vol. 16, No. 3, 220–227, 2001.